Hindawi
Advances in Condensed Matter Physics
Volume 2021, Article ID 5538056, 11 pages
https://doi.org/10.1155/2021/5538056

Research Article

Stress-Driven Evolution on Mismatched $Ca_2Co_2O_5$ Oxide Material: From Geometry to the Electronic States

F. P. Zhang,[1,2,3] **Y. Sun**,[2] **G. L. Zhang**,[3,4] **X. Y. Shi**,[3] **and G. Q. Qin**[3]

[1]*Henan Provincial Engineering Laboratory of Building-Photovoltaics, Institute of Physics, Henan University of Urban Construction, Pingdingshan 467036, Henan, China*
[2]*Department of Physics, Changji University, Changji 831100, China*
[3]*School of Materials Sciences and Engineering, Shijiazhuang Tiedao University, Shijiazhuang 050043, China*
[4]*National Key Laboratory of Advanced Functional Materials, Chinese Ministry of Education, College of Materials Science and Engineering, Beijing University of Technology, Beijing 100124, China*

Correspondence should be addressed to Y. Sun; gghels@gmail.com and G. L. Zhang; zhgl@stdu.edu.cn

Received 2 March 2021; Accepted 26 April 2021; Published 11 May 2021

Academic Editor: Sefer Bora Lisesivdin

The geometrical structures, phase stabilities, electron energy band structures, electron density of states, and atom recombination together with the electron conduction behaviors of the sandwiched $Ca_2Co_2O_5$ with external stress of 1 GPa are intensively studied by the density functional theory method. The studying results show that the symmetry remains undisturbed; the strain to the stress response is anisotropic. The strain of microarchitecture induced by external stress is also anisotropic. There is stronger covalent binding between Co and O. The binding between Co and O within CdI_2 like CoO_2 is very much even covalent, and it is weakened under external stress. But the covalent Co-O binding within the rock salt like CaCoO layer is enhanced. The Ca-O binding strength is insensitive to external stress. An energy gap of 0.1 eV below Fermi level for the spin-up electron band disappears, and the two energy gaps are narrowed for the spin-down electron bands. The p orbital electrons form primarily the bands below Fermi level and the d orbital electrons form primarily the bands above Fermi level. The transitions from p orbital electrons to d orbital electrons produce the conduction. The CdI_2 like CoO_2 layer has been enhanced in terms of participating in the conduction properties with external stress of 1 GPa, and the capability of Co is enhanced while the capability of O is decreased.

1. Introduction

The multioxide framework materials with complicated layered crystal structures such as NaCoO, CaCoO, and BiSrCoO are very much diverse in physical properties, as well as the related sensitivity to structure, spintronics, topology, preparation procedures, and so on [1–6] when compared to pure CoO [Philosophical Magazine 96 (30), 3211–3226]. The family of transitional metal Co-based CaCoO oxide materials which show similar valuable properties are the research focus in recent years. For example, the $Ca_2Co_2O_5$ and $Ca_3Co_4O_9$ type layered oxide materials exhibit especially complex crystal structure, spin topology, preparation variety, and anisotropic transport phenomena [2, 3]. They are similarly composed of rock salts like the CaCoO layer and CdI_2 like the CoO_2 layer that are stacked along c axis with the Sandwich framed crystal structure. The $Ca_2Co_2O_5$ crystalline oxide material was first discovered and reported in terms of its unique sandwiched structure by Vidyasagar et al. in 1984 [4]. Its anisotropic semiconductor conduction and positive temperature-dependent thermopower of $100\,\mu V{\cdot}K^{-1}$ at 100 K were then demonstrated by Funahashi et al. [2, 3]. The $Ca_3Co_4O_9$ crystalline oxide material was discovered and reported in terms of its sandwiched structure and anisotropic transport by Shikano and Funahashi in 2003 [5]. The sensitivity of physical properties to preparation procedures was also investigated during the past years. For instance, the grain alignment together with conduction is very dependent on the external stress of preparation.

The polycrystalline materials of sandwiched CaCoO oxide have been more widely studied in contrast to their single-crystal materials for the sake of preparation cost, fabrication easiness, product scale, etc. In addition, they have been intensively studied experimentally in terms of the transport properties for the intrinsic as well as the regulated materials in recent years [7–11]. In order to recover the performance of single-crystal materials, some fabrication methods have been adopted. For instance, isostatic pressing is one of these ways. In this way, stress ranging from tens of MPas to several GPas is applied to the crystalline bulk materials when preparing. The resulting bulk materials should then be consolidated and regulated with regard to their density and grain alignment in order to get the bulk texture. We have also reported the stress-dependent transport properties of this sandwiched CaCoO crystalline oxide material. The grain alignment and the transport property thereafter can be regulated by external stress ranging from 30 MPa to 500 MPa [9, 12]. The fundamental background physical properties are determined by the geometry structure as well as the electronic states thereafter. The evolution of geometry and electronic states with external stress merits investigation. Unfortunately, a theoretical study in this sandwiched CaCoO crystalline oxide material is moderately lacking.

The transitional metal Cobalt has several d orbital electrons where varieties of spin alignments can be configured. We have demonstrated and reported that the antiferromagnetic aligned $Ca_2Co_2O_5$ crystalline oxide material is most stable among the antiferromagnetic phase and ferromagnetic phase [13]. In the present work, the geometrical structures, microarchitectures, stabilities, electron energy band structures, the electron density of states, and species recombination together with the electron conduction properties of the sandwiched $Ca_2Co_2O_5$ crystalline oxide material with external stress of 1 GPa are intensively studied via the density functional theory (DFT) calculational and analyzing method for the first time to our knowledge.

2. Computational Methods and Details

The sandwiched $Ca_2Co_2O_5$ crystalline oxide material is composed of rock salts like the CaCoO sublayer and CdI_2 like the CoO_2 sublayer along c axis with space group of P1M1. The rock salt like CaCoO and CdI_2 like CoO_2 has the same lattice parameters along b and c axis; their sublattices are mismatched along a axis. The cell angles α, β, and γ are 90°, 90°, and 98.13°, the a, b, and c of the cell are 4.56 Å, 9.66 Å, and 10.84 Å, respectively [2–4]. The schematical crystal structure of this sandwiched $Ca_2Co_2O_5$ crystalline oxide material and the projections onto several planes are shown in Figures 1 and 2.

The present study was carried out based on the platform which is implemented in the Serial Total Energy Package (CASTEP, Cerius2, Molecular Simulation, Inc.) code within the DFT framework [12, 14]. This packaged code is established within the DFT framework which has been successfully applied within the areas of solid states and material sciences for several years [12–14]. The DFT framework has

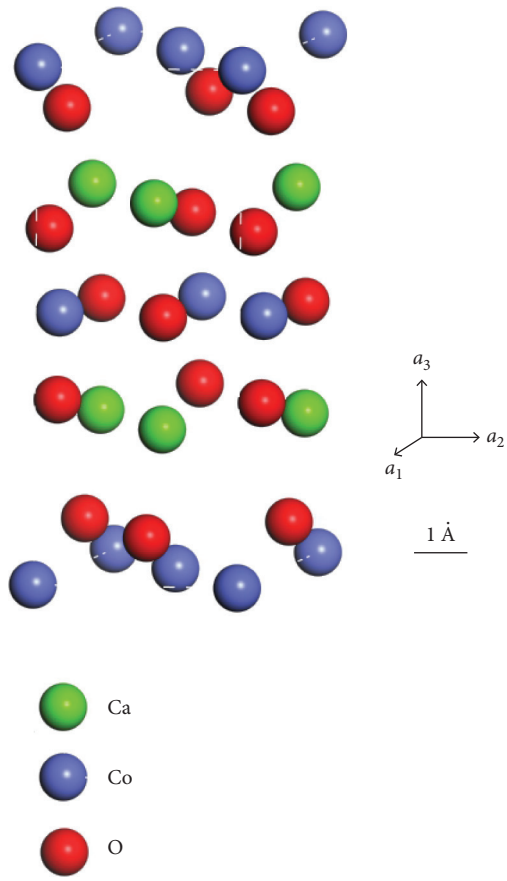

Figure 1: Schematical crystal structure diagram of sandwiched $Ca_2Co_2O_5$ crystalline oxide.

been verified to be one of the most accurate strategies for the solutions of the electronic eigenvalues of solid states [15]. In this work, the deep valance electrons together with the atomic core were treated as Coulombic cores, and the Coulomb interactions of valance electrons with their cores of Ca, Co, and O were herein described by Vanderbilt pseudopotential function. The wave functions of electrons were represented by plane wave functions. The configurations of valence electrons for Ca($3s^2 3p^6 4s^2$), Co($3d^7 4s^2$), and O($2s^2 2p^4$) were selected. The generalized gradient approximation (GGA) scheme and revised Perdew-Burke-Ernzerhof (RPBE) function within the scheme were used to describe the exchange-correlation relation between these electrons. The Hubbard energy revision of 2.5 eV was used to represent the on-site Coulomb effect of Co d electrons. The antiferromagnetic aligned $Ca_2Co_2O_5$ has previously been verified to be most thermally stable among their ferromagnetic phase and antiferromagnetic phase [13]. For the antiferromagnetic phase, the spin state of Co d within the CoO_2 layer was set as contrary as that of Co d within the CaCoO layer for the unpaired electron. In addition, the computational result of the magnetism is well in consistent with the initial settings of the antiferromagnetic phase. In the ground state total energy calculational process, the convergence tolerance of displacement during the self-consistent calculations was set as 0.0005 Å, and the maximum force tolerance was set as 5×10^{-6} eV/atom. The cutoff energy for

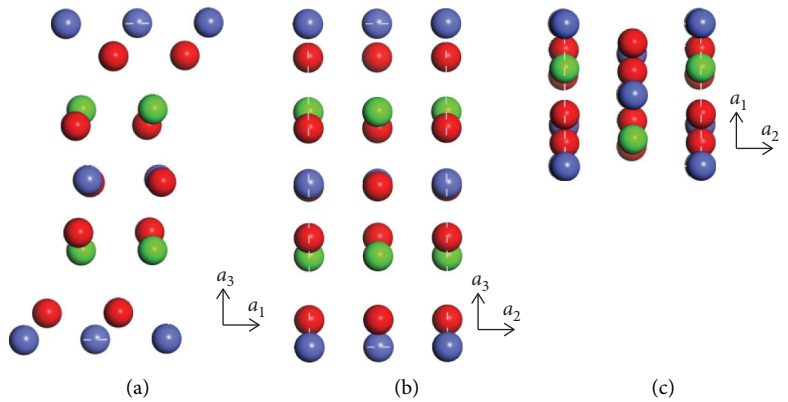

Figure 2: Schematical diagram of sandwiched $Ca_2Co_2O_5$ crystalline oxide for (a) [010] projection, (b) [100] projection, and (c) [001] projection.

electron plane wave expansion of the wave functions was set at 340 eV. The Monkhorst-pack method was used for k point sampling and the k point grid is $1 \times 3 \times 1$. In this work, the computation of schrödinger equation was carried out within the reciprocal space of wave vector sampling for $Ca_2Co_2O_5$ lattice. The electron eigenvalues were deduced and expanded within the first Brillouin zone of the sandwiched $Ca_2Co_2O_5$ crystalline oxide structure as a function of high symmetry points. The first Brillouin zone of the sandwiched $Ca_2Co_2O_5$ crystalline oxide structure and the coordinates of irreducible high symmetry points are shown in Figure 3.

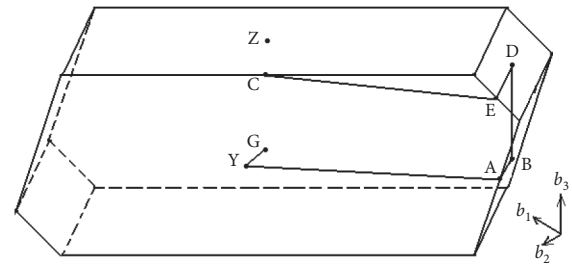

Z (0, 0, 0.5); G (0, 0, 0); Y (0, 0.5, 0); A (−0.5, −0.5, 0); B (−0.5, 0, 0); D (−0.5, 0, 0.5); E (−0.5, 0.5, 0.5); C (0, 0.5, 0.5)

Figure 3: The reduced Brillouin zone and irreducible high symmetry points of sandwiched $Ca_2Co_2O_5$ crystalline oxide.

3. Results and Discussion

Table 1 shows the lattice parameters, total energy E_t, formation enthalpy E_f, and magnetism of sandwiched $Ca_2Co_2O_5$ crystalline oxide material with external stress of 1 GPa, these values for the counterpart $Ca_2Co_2O_5$ are also provided, and the ratios of these parameters are also deduced for comparison. The α, β, and γ keep invariant. The initial lattice symmetry type is not influenced, and the space group remains undisturbed within the externally applied stress range. It can be seen from Table 1 that a, b, c, and cell volume exhibit decreasing trends. This is corresponding to the positive shrinkage expansion of this type of material under external stress. However, it is worth noting that the ratios of a, b, and c between counterpart cells and that under external stress are distinctively different. For example, the ratio of a is 0.997, and the ratio of b and c is 0.998 and 0.999, respectively, corresponding to the disproportionate ratio of the volume of 0.994. It is an indication that the strain induced by external stress is very much anisotropic. Specifically, it can be seen that the strain to the stress response of geometry is sensitive along a direction and insensitive along b c direction for the sandwiched $Ca_2Co_2O_5$ crystalline oxide material. In addition, this is another indication that the bindings within the sandwiched $Ca_2Co_2O_5$ crystalline oxide material are very much different, in terms of the binding nature, binding type, binding length, and binding strength.

It can be seen from Table 1 that the counterpart sandwiched $Ca_2Co_2O_5$ crystalline oxide material without external stress has a total energy of −12556.6 eV for the cell, while the total energy of −12556.5 eV for the cell under external stress is slightly larger than it. Although the difference is negligible, it indicates that the counterpart sandwiched $Ca_2Co_2O_5$ crystalline oxide material without external stress is more thermally stable. In order to verify the stability of the sandwiched $Ca_2Co_2O_5$ crystalline oxide material under different external stress, the formation enthalpy is applied. The formation enthalpy ΔH_{MN} of materials with specific molecular equation $x_M y_N$ can be deduced by

$$\Delta H_{MN} = \frac{E_t - (x_M E_M + y_N E_N)}{x_M + y_N}, \quad (1)$$

where E_t is the total energy of the molecular, E_M and E_N are the averaged energy of element M and N, and x_M and y_N are the quantity of element M and N of the molecular equation. The thermal stability should be higher for material with a smaller formation enthalpy value and it is easier to be formed. It can be seen from Table 1 that the counterpart sandwiched $Ca_2Co_2O_5$ crystalline oxide material has a formation enthalpy of −6.221 eV, which is slightly lower than that under external stress of 1 GPa with −6.220 eV. The counterpart sandwiched $Ca_2Co_2O_5$ crystalline oxide material should be easier to be formed according to the formation enthalpy values. This is in agreement with the total energy that has been discussed above. It is convinced herein that the total energy as well as the formation enthalpy can be applied

Table 1: Lattice parameters, total energy, formation enthalpy, and magnetism of sandwiched $Ca_2Co_2O_5$ crystalline oxide.

	a (Å)	b (Å)	c (Å)	V (Å^3)	α, β (°)	γ (°)	E_t (eV)	E_f (eV)	Magnetism
Counterpart	4.9019	4.5640	11.2403	248.9924	90	98.06	−12556.6	−6.221	AFM
1 GPa	4.8873	4.5536	11.2336	247.5373	90	98.06	−12556.5	−6.220	AFM
Ratio	0.997	0.998	0.999	0.994	1	1	—	—	—

jointly for analyzing the thermal stability of materials; it turns out to be reasonably reliable.

Table 2 shows the binding lengths and binding numbers within sandwiched $Ca_2Co_2O_5$ crystalline oxide material; the binding angles of O-Co-O for the rock salt like CaCoO layer are also provided. Ca and Co act as cationic and O acts as anionic within the crystalline oxide compound, there is Coulomb force, and Ca and Co combine with O thereafter. It can be seen that the distances between Ca and O are larger than those between Co and O in common, indicating their stronger covalent binding effect for Co and O, rather than the Colombian combination trend for Ca and O. This is true with regard to their binding numbers. For example, the binding between Ca and O has binding numbers with values of no more than 0.25, yet the binding between Co and O has binding numbers with values ranging from 0.36 to 0.56, which are distinctively larger. Secondly, it is worth noting that the binding numbers between Co and O within CdI_2 like CoO_2 are obviously larger than those between Co and O within the rock salt like CaCoO layer. In addition, the binding lengths between Co and O within CdI_2 like CoO_2 are obviously shorter than those between Co and O within the rock salt like CaCoO layer. The bindings between Co and O within CdI_2 like CoO_2 are very much covalent than those between Co and O within the rock salt like CaCoO layer. It can be observed from Table 2 that the binding length fluctuations between counterpart $Ca_2Co_2O_5$ and that under external stress of 1 GPa are not proportional. As the external stress is isotropic, so it can be seen that the responses of strain to stress in terms of microarchitechture are not isotropic. It is the same situation for bindings within the rock salt like CaCoO layer as well as the CdI_2 like CoO_2 layer. The binding angle of O-Co-O within the CaCoO layer is increased from 159.610° to 161.355°, indicating the microarchitecture change induced by external stress. Thirdly, it is seen from Table 2 that one of the binding numbers is decreased from 0.53 to 0.52, and the other binding number remains steady for the Co-O binding within the CdI_2 like CoO_2 layer. However, one of the binding numbers is increased from 0.40 to 0.41; other binding numbers remain unchanged for the Co-O binding within the rock salt like CaCoO layer. It can be concluded herein within the external stress range that the covalent Co-O binding within the rock salt like CaCoO layer is enhanced; nevertheless, the covalent Co-O binding within the CdI_2 like CoO_2 layer is weakened. Turn to the Ca-O combinations within the rock salt like CaCoO layer; their binding numbers remain interestingly undisturbed. The Ca-O binding strength is insensitive to external stress and strain within the applied range.

Figure 4 shows the full energy range spin electron band structures of the sandwiched $Ca_2Co_2O_5$ crystalline oxide material with external stress of 1 GPa, the Fermi energy level is relatively set to be 0 eV, and other energy levels are determined thereafter by comparing with Fermi energy level. Figure 5 shows the full energy range spin electron density of states of the sandwiched $Ca_2Co_2O_5$ crystalline oxide material with external stress of 1 GPa. It is true that the bands are anisotropic, especially for a band near the Fermi energy level. It can be seen that the spin-up valence electrons of $Ca_2Co_2O_5$ form five bands within the whole energy range; they locate near −38.5 eV, −19.5 eV, −17 eV, Fermi energy level, and 5 eV. The spin-down valence electrons of $Ca_2Co_2O_5$ form six bands within the whole energy range, and the new band near 1.5 eV can be detected. It can also be observed from Figure 4 that the deep valence bands far from the Fermi level are heavier and the conduction bands are lighter for both of the spin-up and spin-down electrons [13, 14]. There is an obvious band concentration near −19.5 eV, and a strong interaction between electrons can be observed near −2.5 eV, as shown in Figure 5.

Table 2: Binding lengths and binding numbers within sandwiched $Ca_2Co_2O_5$ crystalline oxide.

		0 GPa		1 GPa	
		Length (Å)	Number	Length (Å)	Number
CoO_2 layer	Co-O	1.802	0.53	1.805	0.52
		1.773	0.56	1.772	0.56
CaCoO layer	Co-O	1.879	0.48	1.871	0.48
		1.890	0.47	1.887	0.47
		1.990	0.36	1.994	0.36
		2.328	0.40	2.321	0.41
	Ca-O	2.391	0.10	2.392	0.10
		2.356	0.25	2.349	0.25
		2.384	0.19	2.410	0.19
Angle (°)	O-Co-O	159.610	—	161.355	—

Figure 6 shows the spin electron band structures near the Fermi energy level of the sandwiched $Ca_2Co_2O_5$ crystalline oxide material with external stress of 1 GPa. Figure 7 shows the spin electron density of states near the Fermi energy level of the sandwiched $Ca_2Co_2O_5$ crystalline oxide material with external stress of 1 GPa. For the spin-up electron band structure, a band valley locates at 4.0485 eV and a band peak locates at 1.9680 eV, and there is an indirect energy gap of 2.0805 eV. It has been investigated within our former study that the spin-up band has an energy gap of 2 eV above Fermi level and an energy gap of 0.1 eV below Fermi level for the counterpart $Ca_2Co_2O_5$ crystalline oxide material. The energy gap of 0.1 eV below Fermi level disappears for the $Ca_2Co_2O_5$ crystalline oxide material under external stress of 1 GPa. For the spin-down electron band structure, the band valleys

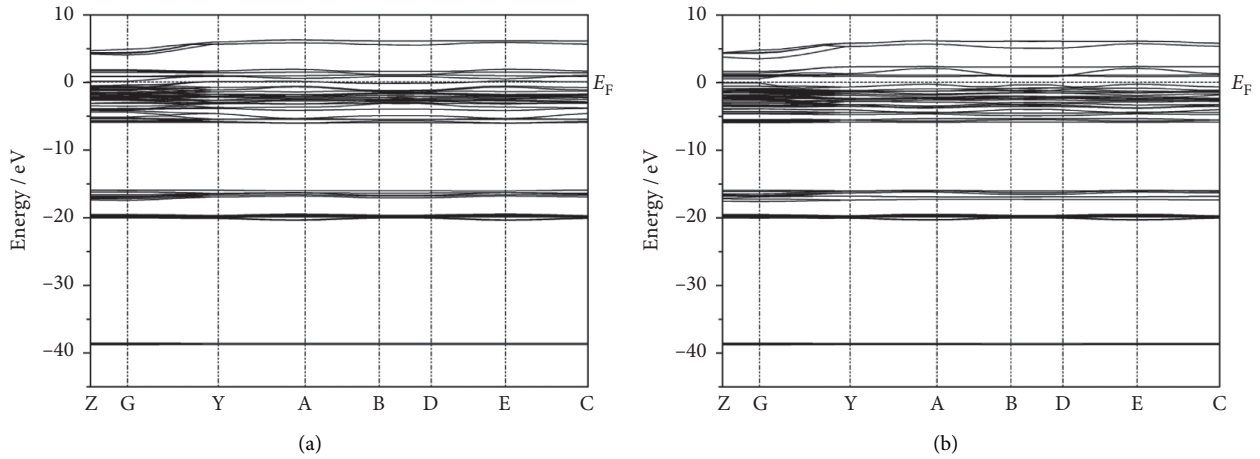

Figure 4: Electron band structures of sandwiched $Ca_2Co_2O_5$ crystalline oxide for (a) spin-up and (b) spin-down.

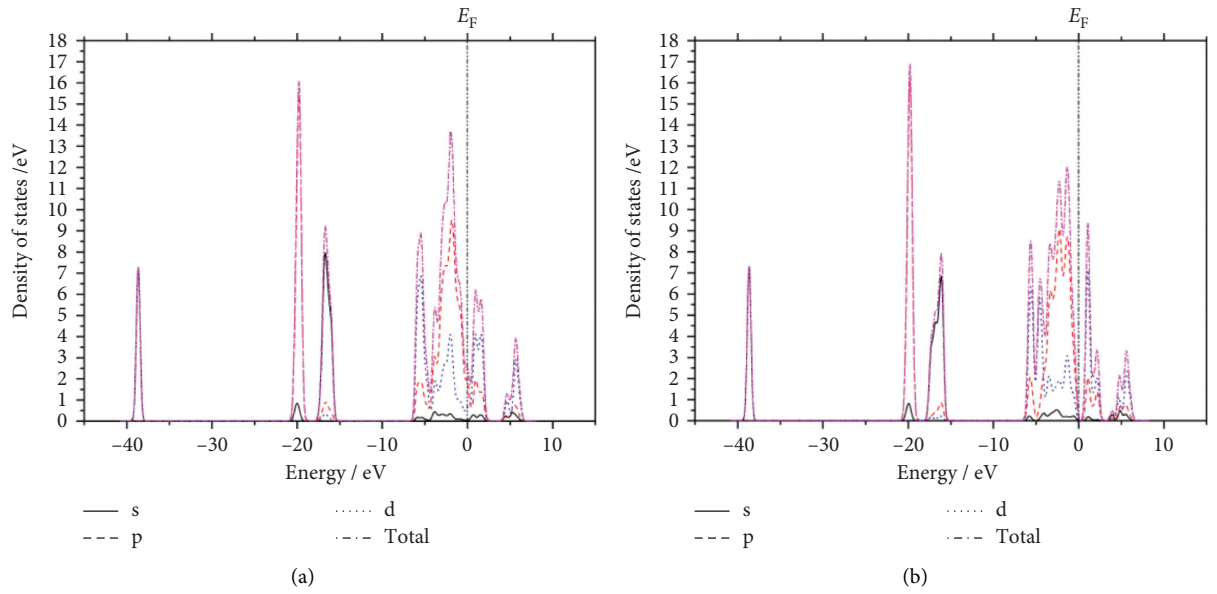

Figure 5: Electron density of states of sandwiched $Ca_2Co_2O_5$ crystalline oxide for (a) spin-up and (b) spin-down.

locate at 3.5112 eV and 0.5647 eV, the band peaks locate at 2.4023 eV and −0.04 eV, and there are two energy gaps of 1.1089 eV and 0.6047 eV. They are indirect gap and direct gap, respectively. It has also been investigated within our former study that the spin-down band has two energy gaps of 0.8 eV and 0.3 eV above the Fermi energy level. The energy gaps are both decreased for the $Ca_2Co_2O_5$ crystalline oxide material under external stress of 1 GPa. It can be seen that energy gaps for both spin-up and spin-down electrons to cross are all narrowed.

It can be seen from Figure 7 that the density of states below Fermi energy level is largely contributed by p orbital electrons and the density of states above Fermi energy level is largely contributed by d state electrons. The p orbital electrons form primarily the bands below Fermi energy level, and the d state electrons form primarily the bands above Fermi energy level. In addition, it can be said that the transitions from p orbital electrons to d orbital electrons should produce the conduction process, and they should be responsible for the electron heat capacity part for this kind of $Ca_2Co_2O_5$ crystalline oxide material.

Figure 8 shows the detailed density of states of the rock salt like CaCoO and CdI_2 like CoO_2 layer near Fermi energy level of the sandwiched $Ca_2Co_2O_5$ crystalline oxide material with external stress of 1 GPa. Figure 9 shows the density of state values on the Fermi energy level for the sandwiched $Ca_2Co_2O_5$, the rock salt like CaCoO, and CdI_2 like CoO_2 layer, as well as species that form these layers. The values marked with number 1 are for the sandwiched $Ca_2Co_2O_5$ crystalline oxide material with external stress of 1 GPa, and the values marked with number 0 are for the intrinsic sandwiched $Ca_2Co_2O_5$ crystalline oxide material with no

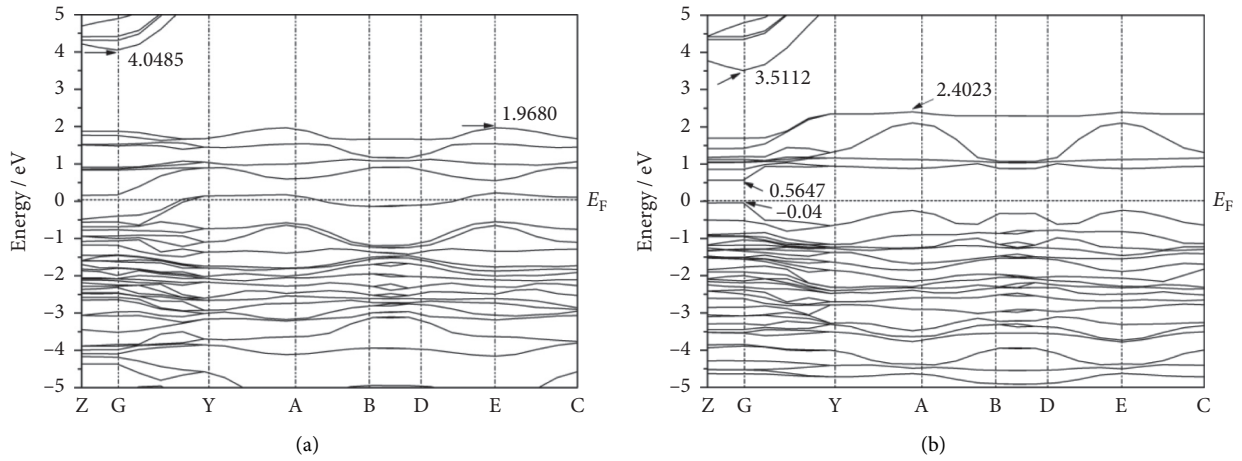

Figure 6: Detailed electron band structures of sandwiched $Ca_2Co_2O_5$ crystalline oxide for (a) spin-up and (b) spin-down.

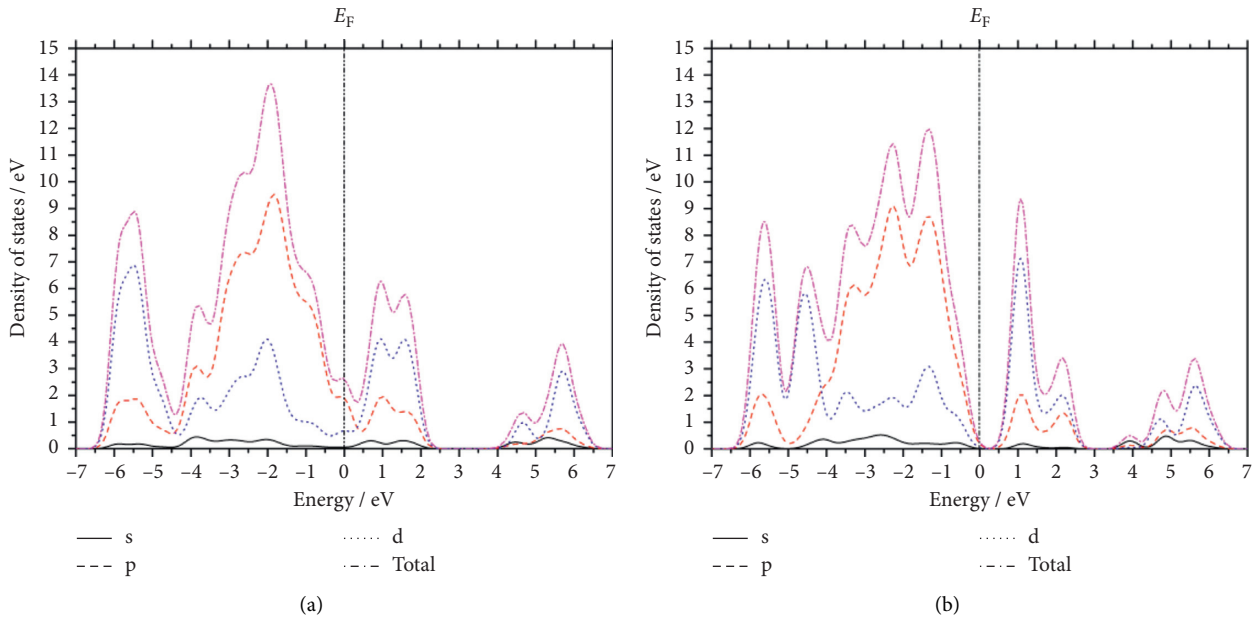

Figure 7: Detailed electron density of states of sandwiched $Ca_2Co_2O_5$ crystalline oxide for (a) spin-up and (b) spin-down.

external stress. It can be seen that the total density of state value for the rock salt like CaCoO layer on Fermi level is 2.3742; it contributes 82% to the total density of state value of 2.8836. So, the total density of the state value portion at Fermi energy level for $Ca_2Co_2O_5$ is also largely composed by the CaCoO layer. Nevertheless, for the intrinsic counterpart $Ca_2Co_2O_5$, the total density of state value for this same layer on the Fermi level is 4.47; it contributes 84% to the total density of state value of 5.31. The proportion of density of states for this layer is decreased from 84% down to 82%. The electronic properties of metallic solids are determined by electrons near Fermi energy; the capability of determining the transport properties is reduced for this layer. It can also be seen that the total density of states value below Fermi energy of this layer is largely composed by p orbital electrons, and the total density of state value above Fermi energy of this layer is largely composed by d orbital electrons. It can be seen that the total density of state value for CdI_2 like CoO_2 layer at Fermi level is 0.5093; it contributes 18% to the total density of state value of 2.8836. Nevertheless, for the intrinsic counterpart $Ca_2Co_2O_5$, the total density of state value for this same layer at Fermi level is 0.83; it contributes 16% to the total density of state value of 5.31. The proportion of density of states for this layer is increased from 16% to 18%. It is seen that this layer has been enhanced in determining the electronic properties. It can also be seen that the total density of states value below Fermi energy of this layer is largely composed by p orbital electrons; the total density of state value above Fermi energy of this layer is largely composed by d orbital electrons.

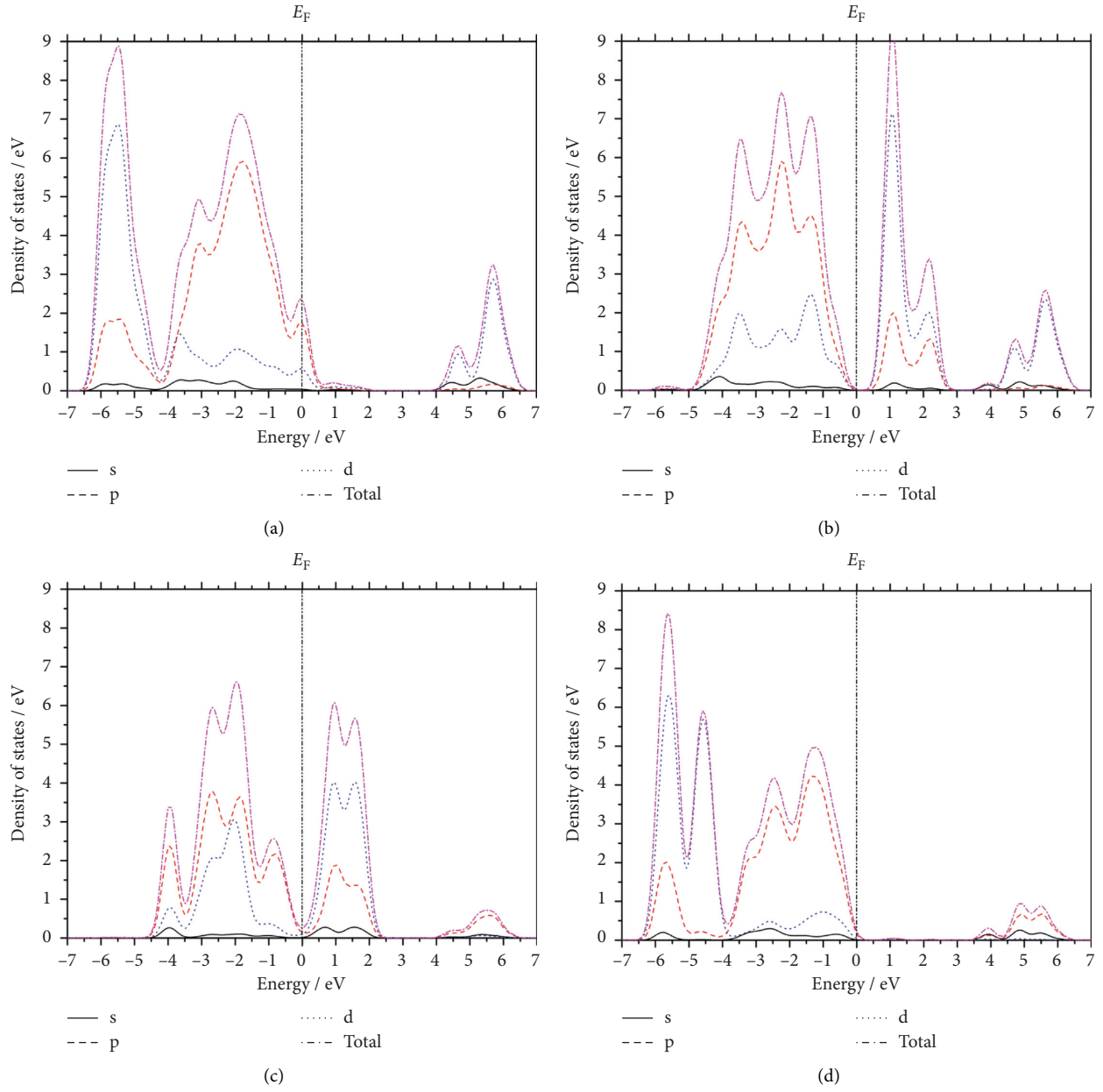

FIGURE 8: Detailed electron density of states of CaCoO layer (a for spin-up and b for spin-down) and CoO_2 layer (c for spin-up and d for spin-down) for sandwiched $Ca_2Co_2O_5$ crystalline oxide.

Figure 10 shows the detailed density of states of Ca, Co, and O within the rock salt like CaCoO near Fermi energy level of the sandwiched $Ca_2Co_2O_5$ crystalline oxide material with external stress of 1 GPa. It is observed that the total density of state values of Ca, Co, and O at Fermi level is 0.0197, 0.565, and 1.7465; they contribute 0.8%, 24%, and 75.2% to the total density of state value of 2.3742 of this layer. Nevertheless, for the counterpart $Ca_2Co_2O_5$, the total density of state values of Ca, Co, and O at the Fermi level is 0.09, 2.08, and 2.30; they contribute 2%, 47%, and 51% to the total density of state value. It can be indicated that the capability of contributing to electronic properties of Ca and Co is decreased; the capability of contributing to electronic properties of O is enhanced. It can be concluded from Figures 9 and 10 that the total density of states of the CaCoO layer at the Fermi energy level is mainly composed of the orbital electrons of Co d and O p. This is the same as the counterpart $Ca_2Co_2O_5$. It is inferred that these two kinds of orbital electrons within this layer contribute to the conduction process.

Figure 11 shows the detailed density of states of Co and O within the CdI_2 like CoO_2 layer near Fermi energy level of the sandwiched $Ca_2Co_2O_5$ crystalline oxide material with external stress of 1 GPa. It is observed that the total density of state values of Co and O at the Fermi level is 0.1854 and 0.3237; they contribute 36% and 64% to the total density of state value of 0.5093 of this layer. However, for the counterpart $Ca_2Co_2O_5$, the total density of state values of Co and

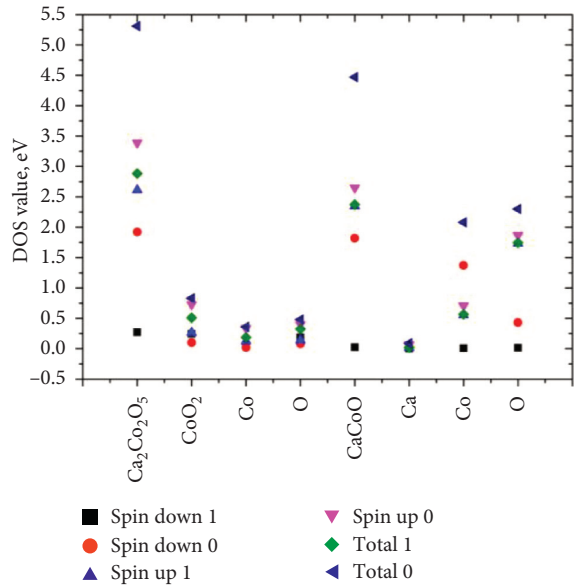

Figure 9: Densities of state values on the Fermi level of the sandwiched $Ca_2Co_2O_5$ crystalline oxide.

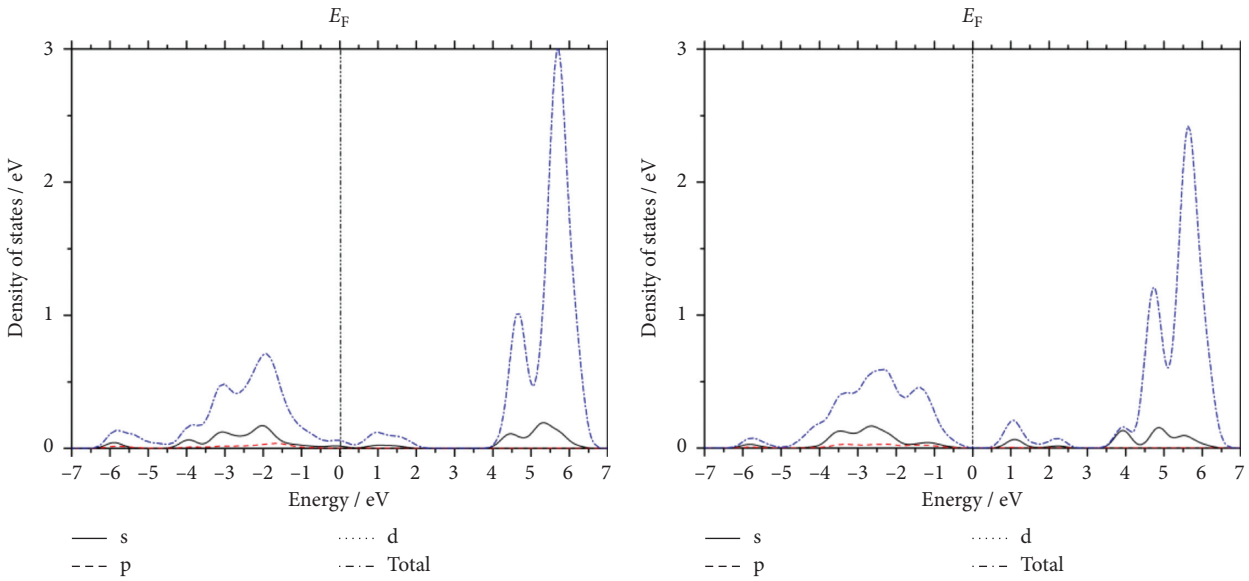

Figure 10: Continued.

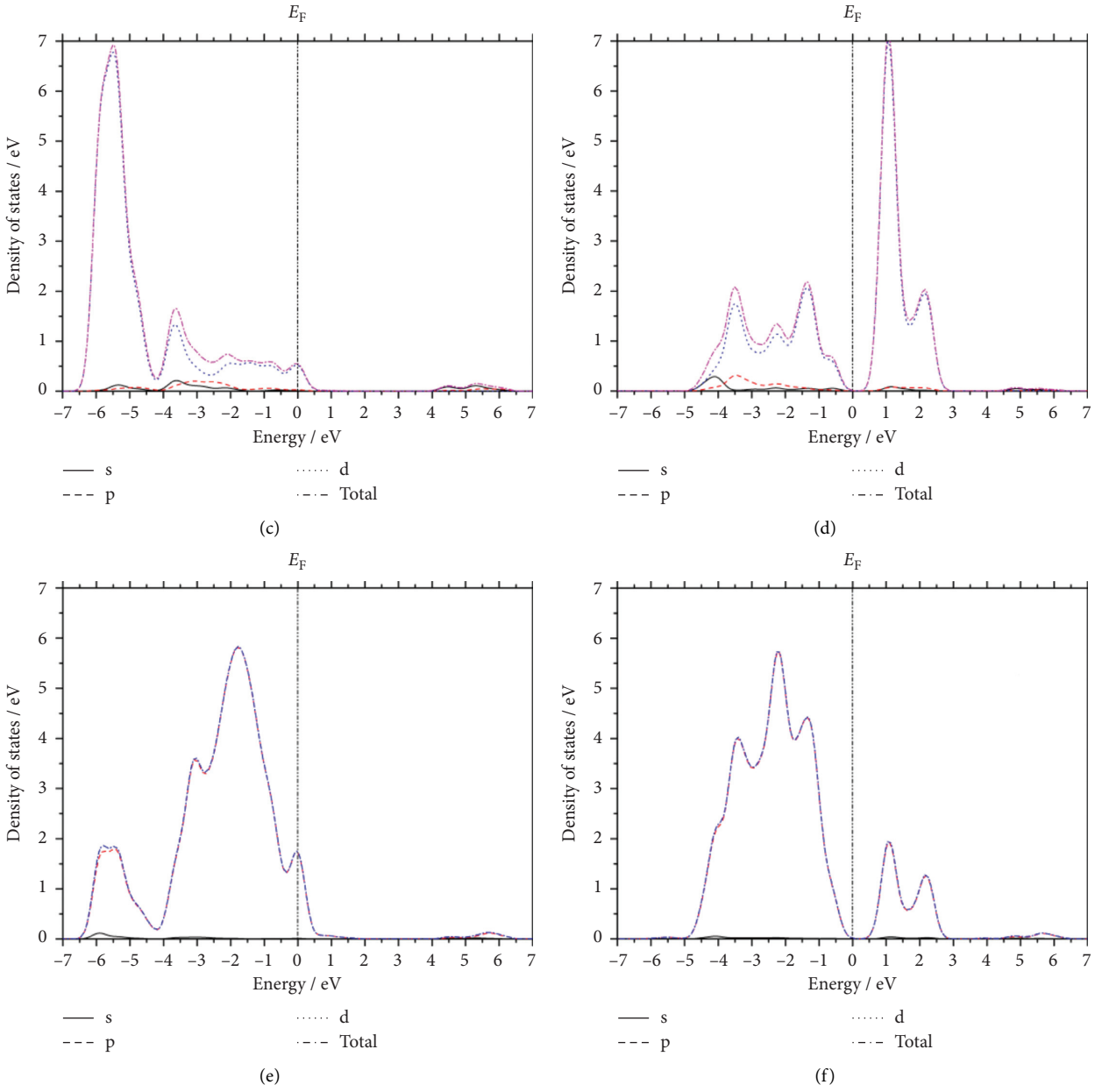

Figure 10: Detailed electron density of states of Ca (a for spin-up and b for spin-down), Co (c for spin-up and d for spin-down), and O (e for spin-up and f for spin-down) for CaCoO layer within sandwiched $Ca_2Co_2O_5$ crystalline oxide.

O at Fermi level is 0.36 and 0.48; they contribute 43% and 57% to the total density of state value of this layer. It can be indicated that the capability of contributing to electronic properties of Co is enhanced; the capability of contributing to electronic properties of O is decreased. It can be concluded from Figures 9–11 that the total density of states of the CaCoO layer at the Fermi energy level is mainly composed of the orbital electrons of Co d and O p, too. This is the

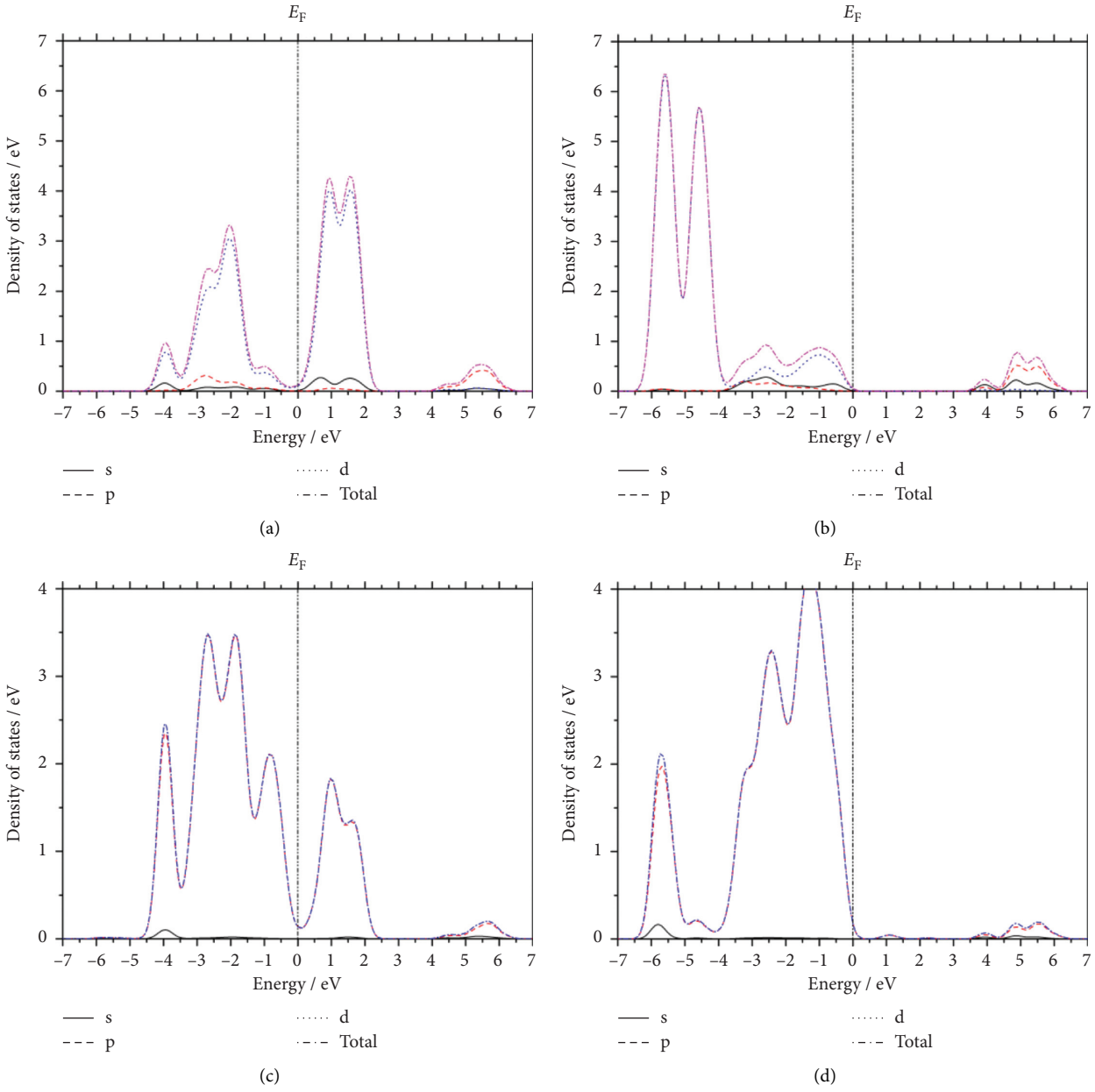

FIGURE 11: Detailed electron density of states of Co (a for spin-up and b for spin-down) and O (c for spin-up and d for spin-down) for CoO_2 layer within sandwiched $Ca_2Co_2O_5$ crystalline oxide.

same as the counterpart $Ca_2Co_2O_5$. It is inferred that these two kinds of orbital electrons within this layer contribute to the conduction process.

4. Conclusions

In conclusion, the geometrical structures, micro-architectures, phase stabilities, electron energy band structures, electron density of states, species recombination, and the electron conduction properties of the sandwiched $Ca_2Co_2O_5$ with external stress of 1 GPa are intensively studied within the framework of density functional theory calculational and analyzing method. The symmetry type is not influenced, and the space group remains undisturbed. The strain-to-stress response of geometry is sensitive along a direction; it is insensitive along the *c* direction. The strain induced by external stress of microarchitecture is anisotropic, indicating the different binding characteristics. The distances between Ca and O are larger than those between Co and O in common, and there is stronger covalent binding for the Co and O. The bindings between Co and O within CdI_2 like CoO_2 are very much covalent than those between Co and O within the rock salt like CaCoO layer. The covalent Co-O binding within the rock salt like CaCoO layer is enhanced; nevertheless, the covalent Co-O binding within the CdI_2 like CoO_2 layer is weakened under the external stress. The Ca-O binding strength is insensitive to external stress. The intrinsic sandwiched $Ca_2Co_2O_5$ is more stable.

An energy gap of 0.1 eV below Fermi level for spin-up electron band disappears, and the two energy gaps are decreased to 1.1089 eV and 0.6047 eV for the spin-down electron bands, respectively. The p orbital electrons form largely the bands below Fermi energy level and the d state electrons form largely the bands above Fermi energy level. The transitions from p orbital electrons to d orbital electrons produce the conduction process. The CdI_2 like CoO_2 layer has been enhanced in terms of involving the transport properties with external stress of 1 GPa. Nevertheless, the rock salt like the CaCoO layer exhibits contrary characteristics. For the CdI_2 like CoO_2 layer, the capability of contributing to transport properties for Co is enhanced, but the capability of contributing to transport properties for O is decreased. For the rock salt like the CaCoO layer, the capability of contributing to transport properties for Ca and Co is decreased; the capability of contributing to transport properties for O is enhanced.

Data Availability

The data used to support the findings of this study are available from the corresponding author upon request.

Conflicts of Interest

The authors declare no conflicts of interest.

Acknowledgments

The authors would like to thank the support provided by the Henan Provincial Natural Science Foundation under grant no. 162300410007. The fruitful discussions on band formation and related electron alignments with Prof. J. J. Zhao and Dr. S. J. Qin are also acknowledged.

References

[1] S. Walia, S. Balendhran, H. Nili et al., "Transition metal oxides-thermoelectric properties," *Progress in Materials Science*, vol. 58, no. 8, pp. 1443–1489, 2013.

[2] R. Funahashi, I. Matsubara, H. Ikuta, T. Takeuchi, U. Mizutani, and S. Sodeoka, "An oxide single crystal with high thermoelectric performance in air," *Japanese Journal of Applied Physics*, vol. 39, no. 11, pp. L1127–L1129, 2000.

[3] S. Funahashi, T. Nakamura, K. Kageyama, and H. Ieki, "Monolithic oxide-metal composite thermoelectric generators for energy harvesting," *Journal of Applied Physics*, vol. 109, no. 12, p. 124509, 2011.

[4] K. Vidyasagar, J. Gopalakrishnan, and C. N. R. Rao, "A convenient route for the synthesis of complex metal oxides employing solid-solution precursors," *Inorganic Chemistry*, vol. 23, no. 9, pp. 1206–1210, 1984.

[5] M. Shikano and R. Funahashi, "Electrical and thermal properties of single-crystalline (Ca_2CoO_3) $0.7CoO_2$ with a $Ca_3Co_4O_9$ structure," *Applied Physics Letters*, vol. 82, no. 12, pp. 1851–1853, 2003.

[6] A. C. Masset, C. Michel, A. Maignan et al., "Misfit-layered cobaltite with an anisotropic giant magnetoresistance: $Ca_3Co_4O_9$," *Physical Review B*, vol. 62, no. 1, pp. 166–175, 2000.

[7] S. Li, R. Funahashi, I. Matsubara, K. Ueno, S. Sodeoka, and H. Yamada, "Thermoelectric properties of oxides of $Ca_2Co_2O_5$ with bi substitution," *Journal of Materials Science Letters*, vol. 19, no. 15, pp. 1339–1341, 2000.

[8] P. S. Liu, G. Chen, J. Pei et al., "Preparation and characterization of the new oxides $Ca_2{-}xNa_xCo_2O_5$," *Physica B: Condensed Matter*, vol. 403, no. 10-11, pp. 1808–1812, 2008.

[9] Y. Zhang, J. Zhang, and Q. Lu, "Rapid synthesis of $Ca_2Co_2O_5$ textured ceramics by coprecipitation method and spark plasma sintering," *Journal of Alloys and Compounds*, vol. 399, no. 1-2, pp. 64–68, 2005.

[10] J. Lan, Y.-H. Lin, G.-J. Li et al., "High-temperature electrical transport behaviors of the layered $Ca_2Co_2O_5$-based ceramics," *Applied Physics Letters*, vol. 96, no. 19, p. 192104, 2010.

[11] J. Pei, G. Chen, X. Li, Y. X. Li, and N. Zhou, "Molten salt synthesis and thermoelectric properties of $Ca_2Co_2O_5$," *Materials Letters*, vol. 63, no. 17, pp. 1459–1461, 2009.

[12] F. P. Zhang, J. L. Shi, J. W. Zhang, X. Y. Yang, and J. X. Zhang, "Grain alignment modulation and observed electrical transport properties of $Ca_3Co_4O_9$ ceramics," *Results in Physics*, vol. 12, p. 321, 2019.

[13] F. P. Zhang, G. L. Zhang, G. Q. Qin, S. J. Qin, and J. X. Zhang, "Electronic states and observed anisotropic band structure of $Ca_2Co_2O_5$ type layered compound: a comprehensive study," *Results in Physics*, vol. 15, p. 102739, 2019.

[14] Y.-Q. Zhao, L.-J. Wu, B. Liu, L.-Z. Wang, P.-B. He, and M.-Q. Cai, "Tuning superior solar cell performance of carrier mobility and absorption in perovskite $CH_3NH_3GeCl_3$: a density functional calculations," *Journal of Power Sources*, vol. 313, pp. 96–103, 2016.

[15] A. H. Reshak, "Spin-polarized second harmonic generation from the antiferromagnetic CaCoSO single crystal," *Scientific Reports*, vol. 7, p. 46415, 2017.